Atmos. Chem. Phys. Discuss., 15, 7239–7266, 2015
www.atmos-chem-phys-discuss.net/15/7239/2015/
doi:10.5194/acpd-15-7239-2015

Atmospheric Chemistry and Physics Discussions

A simple formulation of the CH_2O photolysis quantum yields

E.-P. Röth[1] **and D. H. Ehhalt**[2]

[1]Institute for Energy and Climate Research (IEK-7: Stratosphere), Research Center Jülich, Jülich, Germany
[2]Institute for Energy and Climate Research (IEK-8: Troposphere), Research Center Jülich, Jülich, Germany

Received: 19 January 2015 – Accepted: 12 February 2015 – Published: 10 March 2015

Correspondence to: E.-P. Röth (e.p.roeth@fz-juelich.de)

Published by Copernicus Publications on behalf of the European Geosciences Union.

Abstract

New expressions for the various wavelength – dependent photolysis quantum yields of CH_2O, Φ_j, are presented. They are based on combinations of functions of the type $A_i/(1+\exp[-(1/\lambda - 1/\lambda_{0i})/b_i])$. The parameters A_i, b_i, and λ_{0i} which have a physical meaning are obtained by fits to the measured data of the Φj_i available from the literature. The altitude dependence of the photolysis frequencies resulting from the new quantum yield expressions are compared to those derived from the Φ_j recommended by JPL and IUPAC.

1 Introduction

Formaldehyde, CH_2O, is an important trace gas in the atmosphere. It is formed as an intermediate in the oxidation of methane and non-methane hydrocarbons, and destroyed by the reaction with OH and by photolysis in the near ultraviolet. The photolysis involves several channels. Following the excitation (Reaction R1), CH_2O^* can decay into purely molecular products (Reaction R2), or into products that in the atmosphere lead to the eventual formation of hydroperoxy radicals, HO_2, (Reactions R3 and R4). The quenching Reaction (R5) and fluorescence (Reaction R6) can influence the quantum yields of the product channels.

$$CH_2O + h\nu \rightarrow CH_2O^* \quad \text{(R1)}$$
$$CH_2O^* \rightarrow CO + H_2 \quad \text{(R2)}$$
$$CH_2O^* \rightarrow CHO + H \quad \text{(R3)}$$
$$CH_2O^* \rightarrow CO + H + H \quad \text{(R4)}$$
$$CH_2O^* + M \rightarrow CH_2O + M^{\#} \quad \text{(R5)}$$
$$CH_2O^* \rightarrow CH_2O + h\nu' \quad \text{(R6)}$$

As it turns out the molecular channel, Reaction (R2), provides the by far largest source of molecular hydrogen, H_2, in the atmosphere (Ehhalt and Rohrer, 2009). The radical channels, Reactions (R3) and (R4), that generate HO_2 radicals, enhance local photochemistry. Finally each destruction of a CH_2O molecule – including that by OH – eventually results in a carbon monoxide molecule, CO. As a consequence CH_2O is also an important source of CO in the atmosphere.

Recognizing the importance for atmospheric chemistry the quantum yields of the CH_2O photolysis were measured early on and by various authors (see Sander et al., 2011; Atkinson et al., 2006, and the internet version IUPAC (2013) for summaries).

The quantum yield Φ_{mol} of the molecular branch (Reaction R2) was usually measured by monitoring the H_2 production while scavenging the H atoms to prevent their contribution to the H_2 production (e.g. Moortgat et al., 1978; Horowitz and Calvert, 1978). The formation of the molecular products via the reaction path of a roaming H atom (see e.g. Bowman and Shepler, 2011; and Christoffel and Bowman, 2009) was not known then and is not included explicitly in our list of reactions but it is included in Reaction (R2), and its quantum yield is part of the measured Φ_{mol}.

Reactions (R3) and (R4) form the radical channel with the combined quantum yield Φ_{rad} which in some cases was investigated directly by measuring the products, H and CHO (e.g. Smith et al., 2002; Gorrotxategi et al., 2008; Tatum Ernest et al., 2012).

The fluorescence quantum yield (Reaction R6) was measured by Miller and Lee, 1978, in the wavelength range 290 to 360 nm. Its maximum at 353 nm is less than 3.5 % and it is less than 1 % at the other wavelengths considered. It will, therefore, be neglected here. We know of no measurements below 290 nm.

The total quantum yield Φ_{tot}, i.e. the fraction of the decay of excited formaldehyde, CH_2O^*, into products other than its ground state, was derived from the CO production. By definition Φ_{tot} is the sum of the quantum yields of the molecular and the radical channel:

$$\Phi_{tot} = \Phi_{mol} + \Phi_{rad} \tag{1}$$

The measured wavelength dependences of the quantum yields are usually given in tabular form (see e.g. Atkinson et al., 2006; IUPAC, 2013) or as a fit by a fourth order polynomial (see Sander et al., 2011). To provide a more handy tool for atmospheric modeling we propose to use combinations of energy dependent functions of the type

$$\frac{A}{1 + \exp\left[\frac{-(1/\lambda - 1/\lambda_0)}{b}\right]} \tag{2}$$

to fit Φ_{mol} and Φ_{rad}. These functions are well-suited to map smooth transitions. They allow to include pressure and temperature dependences. And the resulting parameters are few and have a physical meaning: in particular $1/\lambda_0$ corresponds to the threshold energy of the respective reaction; b describes the width of the transitions. Moreover, the formalism should also provide a useful template for the formulation of the analogous Φ_i for the isotopologues of formaldehyde.

Our analysis of the quantum yields will be based on the data filed by JPL (Sander et al., 2011) and IUPAC (2006) omitting all measurements with an obvious bias. Likewise, only publications of independent measurements were taken into account, i.e. if measured data appear in several publications by the same authors, only the latest data were considered.

First, in Sects. 2 to 4, we will fit the measured wavelength dependences of the various Φ separately and compare them to those reported in the literature. In a second step, after having convinced ourselves that the parameters from the separate fits that should correspond to each other are indeed similar in value, we attempt a simultaneous fit of all Φ in Sect. 5.

2 The quantum yield of the radical channel

Most publications on the formaldehyde photolysis deal with the radical channel (Reaction R3) – notably: Horowitz and Calvert (1978), Moortgat et al. (1983), Smith

et al. (2002), Gorrotxategi et al. (2008), and Tatum Ernest et al. (2012). Nearly all of these measurements were made at room temperature, and experiments and theory indicate that there is no pressure dependence of Φ_{rad}. We, therefore, assume all these data to be comparable and their variance attributable to experimental error. Thus all these data are combined in Fig. 1 without any weighing. Smith et al. (2002) attributed some of the variance in their data to a line structure in Φ_{rad}. The possibility of a line structure appears corroborated by the data of Tatum Ernest et al. (2012), which show a strong feature in Φ_{rad} at 321 nm. For comparison the data of Tatum Ernest et al. are also shown in Fig. 1, but they are not used for the fit.

To fit the experimentally observed wavelength dependence of Φ_{rad} we use a combination of two functions of the type mentioned above, one for the decay of Φ_{rad} to longer wavelengths at about 328 nm, the other for the decay towards shorter wavelenghts at 277 nm. To obtain the fit parameters and their errors a simplex algorithm (Nelder and Mead, 1965) is used in combination with a bootstrapping method with 2000 arbitrary removals of 20 % of the data. The result is given by Eq. (3), with λ in nm:

$$\Phi_{rad} = \frac{0.72}{1 + \exp\left(\frac{-(1/\lambda - 1/328.0)}{5.2\times10^{-5}}\right)} - \frac{0.38}{1 + \exp\left(\frac{-(1/\lambda - 1/278.4)}{4.7\times10^{-5}}\right)} \quad (3)$$

It is also shown in Fig. 1.

Equation (3) holds primarily for room temperature. The respective parameters will be labelled by the subscripts l, s. The λ_0 mark the inflection points in the decays: $\lambda_{0,l} = 328.0$ nm; $\lambda_{0,s} = 278.4$ nm. The corresponding b define the wavelength interval within which the decrease takes place. Owing to the scatter in the measured Φ_{rad} data all these parameters exhibit an uncertainty range. The estimated 1σ errors are listed in Table 1 along with the values of the parameters. We note that $\lambda_{0,l}$ closely corresponds to the dissociation energy of the H-CHO bond namely 30328.5 cm^{-1} or 329.7 nm (Terentis et al., 1998) and that $\lambda_{0,s}$ approximately corresponds to the heat of formation of Reaction (R4) namely 423 kJ mol^{-1} or 283 nm (Sander et al., 2011).

Moortgat et al. (1983) have also measured the wavelength dependence of Φ_{rad} at 220 K. Given the experimental variance in those admittedly sparse data, Eq. (3) also fits the measured Φ_{rad} at 220 K quite well (not shown here). Thus, as far as the experimental data on Φ_{rad} are concerned, Eq. (3) covers the temperature range of 220 to 300 K relevant for atmospheric modeling and there is no immediate need to introduce a temperature dependence. On the other hand, theoretical considerations suggest the inclusion of the internal energy of the CH_2O molecule, and this can be easily done: following Troe (2007) one can add a term 3kT (appropriately scaled) to $1/\lambda$ in the left hand term of Eq. (3). In Sect. 5, Discussion, we will investigate the impact of this T dependence (see Eq. 12) on the altitude profile of the respective photolysis frequency. In principle, another weak T dependence can arise through the parameter b. That dependence could be easily accommodated by replacing b by $(b_0 + b_1 T)$ should future Φ_{rad} measurements provide enough information to warrant such a step.

The present formulation of Eq. (3) with constant parameters b – i.e. b independent of λ – forces the decrease to be nearly symmetrical around the respective λ_0. This is not necessarily realistic. Again, if future measurements or theoretical considerations should prove the need, an asymmetry could be easily accommodated by allowing b to depend on λ.

Finally, we note, that a line structure could be superimposed on Eq. (3) without difficulty. For the moment we refrain from doing so for two reasons. (1) As Tatum Ernest et al. (2012) showed even the strong feature in Φ_{rad} at 321 nm would change the photolysis frequency in the atmosphere, j_{rad}, by only −4 %, because it coincides with a strong minimum in the absorption coefficient of CH_2O. Thus the error possibly introduced by its neglect is comparatively small (see discussion below). (2) The measurements of Φ_{rad} by Smith et al. (2002), and Gorrotxategi et al. (2008) contain data points close to 321 nm which fall right on the average Φ_{rad} given by Eq. (3). They were made with sufficient resolution to resolve the feature at 321 nm and are therefore somewhat at variance with the finding of Tatum Ernest et al. (2012).

Figure 1 also contains the recommended wavelength dependences of Φ_{rad} given in the evaluations by JPL (Sander et al., 2011) and IUPAC (2006). The reason for the choice of IUPAC (2006) over IUPAC (2013) is that the former data, which were first published in 2002 and remained in the internet until 2012, had many users in the past and possibly still has at present. Further included is the theory-based dependence derived by Troe (2007); it covers only the restricted wavelength range from 310 to 350 nm. As a quantitative measure of the quality of these fits we here add the coefficient of determination c. In the present case this is identical to the correlation coefficient between fitted and measured data. These correlation coefficients are: $c = 0.821$ (IUPAC, 2006); $c = 0.840$ (Troe, 2007); $c = 0.898$ (JPL, 2011); and $c = 0.905$ (this work); that is the quality of these various fits does not differ drastically.

3 The total quantum yield

There are more direct measurements for Φ_{tot} and its dependence on λ than for Φ_{mol}. To obtain higher accuracy we, therefore, first obtain a fit for $\Phi_{tot}(\lambda)$ and then use Eq. (1), i.e. $\Phi_{mol} = \Phi_{tot} - \Phi_{rad}$ for a fit of $\Phi_{mol}(\lambda)$. That fit is later compared to the measured dependence of Φ_{mol} on λ.

The available measurements of $\Phi_{tot}(\lambda)$ at 300 K temperature and 1013 hPa pressure are reproduced in Fig. 2. The values of Φ_{tot} at 355 and 353 nm were obtained by interpolating the respective Stern–Volmer plots given by Moortgat et al. (1979, 1983) to the pressure of 1 atm. The Φ_{tot} values at $\lambda < 340$ nm are pressure independent. The measured $\Phi_{tot}(\lambda)$ exhibits three regions: a plateau between 290 and 330 nm, a steep decrease to zero at longer wavelengths, and a weak decrease to $\Phi_{tot} \sim 0.8$ at shorter wavelengths. The average measured Φ_{tot} in the plateau is 1.06 ± 0.09 – not significantly different from 1 – the maximum possible value. Therefore, in the fit we will fix this value to unity. The separation of the two decreases by a plateau with $\Phi_{tot} = 1$ also means that it is possible to fit these two regions of decrease separately and independently of each other.

The measurements in Fig. 1 indicate that Φ_{rad} vanishes at $\lambda > 340$ nm; at those wavelengths Φ_{tot} becomes identical to Φ_{mol}. Moreover, tunneling processes extend the photolysis of CH_2O to H_2 and CO well beyond the threshold energy of about 350 nm (Troe, 2007). In this energy regime the rate of decay into the molecular channel decreases to values where collisional quenching of the excited formaldehyde molecule (Reaction R5) begins to compete. Consequently, Φ_{mol} and Φ_{tot} become pressure dependent. Based on theoretical modeling and comparison with the data of Moortgat et al. (1978, 1983), Troe (2007) proposed a Stern–Volmer formulation for Φ_{mol} for $\lambda > 340$ nm:

$$\Phi_{mol} = \frac{1}{1 + 1.4 \exp\left(c\left(\lambda - \lambda_0\right)\right)\left(M/M_0\right)} \quad (4)$$

with $\lambda_0 = 349$ nm; $c = 0.225\,\mathrm{nm}^{-1}$ for $\lambda > \lambda_0$ and $c = 0.205\,\mathrm{nm}^{-1}$ for $\lambda < \lambda_0$ and M the number density of the bath gas. $M_0 = 2.46 \times 10^{19}\,\mathrm{cm}^{-3}$, the number density at 1013 hPa pressure and 300 K temperature. Troe (2007) also pointed out that on theoretical grounds the temperature dependence of Φ_{mol} should be small compared to the experimental uncertainties and thus negligible at this stage. This is somewhat at variance to the measurements by Moortgat et al. (1983) which seem to indicate such a dependency, albeit with large uncertainties.

Since Φ_{tot} equals Φ_{mol} for $\lambda > 340$ nm where nearly all of the change in Φ_{tot} with wavelength is located, and since Eq. (4) approaches unity for $\lambda < 330$ nm, Eq. (4) should also provide a good approximation for $\Phi_{tot}(\lambda)$. In fact we could use it with its current parameters as our intended fit (see Fig. 2).

However, we prefer to formulate our fit in terms of energy, i.e. $1/\lambda$. Moreover, a direct fit to the data in Fig. 2 will merge the pre-exponential factor in Eq. (4) with λ_0. So, instead of using Eq. (4) we will fit Eq. (5) to the data at $\lambda > 310$ nm in Fig. 2:

$$\Phi_{tot} = \frac{1}{1 + \exp\left(\frac{-\left(1/\lambda - 1/\lambda_{0,l}\right)}{b_l}\right) \cdot \left(M/M_0\right)} \quad (5)$$

Our fit yields the parameters $\lambda_{0,l}$ and b_l of Table 2. In this case $\lambda_{0,l}$ has a somewhat different meaning than before. Here, $\lambda_{0,l}$ not only depends on the threshold energy of the reaction involved, but also on the quenching efficiency with which energy is drained from the excited CH_2O molecule. But as before $\lambda_{0,l}$ represents the inflection point in the decrease of Φ, at least for $M = M_0$.

The fit of Φ_{tot} for the short wave decrease relies on our model Eq. (2) and yields the parameters listed in Table 2.

The equation for $\Phi_{tot}(\lambda)$ over the full wavelength range therefore is:

$$\Phi_{tot} = \frac{1}{1 + \exp\left(\frac{-(1/\lambda - 1/347.1)}{5.7\times10^{-5}}\right)(M/M_0)} - \frac{0.20}{1 + \exp\left(\frac{-(1/\lambda - 1/284.3)}{3.5\times10^{-5}}\right)} \quad (6)$$

with λ given in nm.

We have not been able to find a ready explanation for the experimentally observed weak decrease of Φ_{tot} at shorter wavelengths in the literature. We note, however, that $\lambda_{0,s}$ = 284.3 corresponds closely to the heat of formation for reaction Eq. (4) (see Sect. 2).

Following the arguments by Troe (2007) we assume the temperature dependence of $\Phi_{tot}(\lambda)$ to be negligible. But here again, our fitting functions could readily be modified to include a T dependence.

$\Phi_{tot}(\lambda)$ from Eq. (6) is also shown in Fig. 2. It compares favorably to the measured data of Φ_{tot}. For additional comparison Fig. 2 also contains the recommended wavelength dependences of Φ_{tot} given in the evaluations by JPL (Sander et al., 2011) and IUPAC (2006). Further included is the dependence derived from Troe's (2007) Φ_{mol}; it covers only the restricted wavelength range from 310 to 370 nm. Just as Eq. (6), the $\Phi_{tot}(\lambda)$ from JPL and that based on Troe (2007) agree well with the measurements. An exception are the recommended values from IUPAC (2006) which clearly deviate from the measurements in the range 330 nm < λ < 350 nm. The consequence of this deviation on the coefficient of determination is relatively small: c = 0.913, whereas the

others are: JPL, c = 0.959; Troe, c = 0.944; present, c = 0.956. In IUPAC (2013) this deviation is removed; the corresponding c is 0.924.

4 The quantum yield of the molecular channel

Since Φ_{mol} is given by $\Phi_{tot} - \Phi_{rad}$, it could be simply obtained from the difference of Eqs. (6) and (3). Explicitly:

$$\Phi_{mol} = \Phi_{tot} - \Phi_{rad} = \frac{1}{1 + \exp\left(\frac{-(1/\lambda - 1/347.1)}{5.7\times10^{-5}}\right)(M/M_0)} - \frac{0.20}{1 + \exp\left(\frac{-(1/\lambda - 1/284.3)}{3.5\times10^{-5}}\right)} - \frac{0.72}{1 + \exp\left(\frac{-(1/\lambda - 1/328.0)}{5.2\times10^{-5}}\right)} + \frac{0.38}{1 + \exp\left(\frac{-(1/\lambda - 1/278.4)}{4.7\times10^{-5}}\right)} \quad (7)$$

On the other hand Φ_{mol} can be obtained by a direct fit to the measured data. This requires a combination of only three functions of the Eq. (2) type and the fit results in:

$$\Phi_{mol} = \frac{1}{1 + \exp\left(\frac{-(1/\lambda - 1/345.2)}{6.2\times10^{-5}}\right)(M/M_0)} - \frac{0.75}{1 + \exp\left(\frac{-(1/\lambda - 1/325.3)}{3.9\times10^{-5}}\right)} + \frac{0.24}{1 + \exp\left(\frac{-(1/\lambda - 1/274.2)}{2.3\times10^{-5}}\right)} \quad (8)$$

Equation (8) makes the implicit assumption that the short wave decreases in Φ_{tot} and Φ_{rad} (second and fourth term in Eq. 7) have the same $\lambda_{0,s}$ and b_s. The estimated 1σ errors along with the fit parameters are listed in Table 3.

In Fig. 3 $\Phi_{mol}(\lambda)$ from Eq. (8) is compared to the measured data on $\Phi_{mol}(\lambda)$. The latter consist of direct measurements of Φ_{mol} by Moortgat et al. (1979, 1983), and data

based on measured Φ_{tot} and Φ_{rad} by Horowitz and Calvert (1978). The agreement of Eq. (8) with the measurements is quite reasonable. For further comparison Fig. 3 also includes the recommendations by JPL (Sander et al., 2011) and IUPAC (2006) as well as a fit based on Φ_{tot} and Φ_{rad} derived from Troe (2007). The respective coefficients of determination are: c = 0.822 (IUPAC, 2006); c = 0.838 (Troe, 2007); c = 0.947 (JPL; 2011); c = 0.958 (this work); IUPAC (2013) would yield c = 0.843.

5 Simultaneous fit of Φ_{rad}, Φ_{mol}, and Φ_{tot}

A comparison of the parameters and their errors obtained from the individual fits of the various Φ suggests that the $\lambda_{0,s}$, $\lambda_{0,m}$, $\lambda_{0,l}$ and b_s, b_m, b_l in a given fit equation do not differ significantly from the corresponding parameters in the others. We, therefore, felt justified to attempt a simultaneous fit of all Φ. In this attempt we assume that the corresponding λ_0 and b parameters in the various equations for Φ are indeed identical. We further assume that Φ_{tot} reaches a maximum value of 1 and that Eq. (1) holds. With these assumptions the total number of fit parameters for all three Φ together reduces to 9. The simultaneous calculation of the 9 unknown parameters results in the equations for the Φ_j listed in Table 4, The coefficients of determination together with the function parameters and their estimated 1σ errors are tabulated in Table 5.

The functions of Table 4 differ somewhat, but hardly significantly, from those given by Eqs. (3), (6), and (8) considering the experimental uncertainties. The coefficients of determination are comparable to those from the individual fits. Because of their simplicity Eqs. (11)–(13) represent our preferred formulation of the CH_2O quantum yields and will be used in the discussion below.

6 Discussion

In the foregoing sections we presented new formulations of Φ_{tot}, Φ_{rad}, and Φ_{mol} for CH_2O. The presentation also made it clear that there is room for improvements. One

concerns the temperature dependence of Φ. Given the experimental uncertainties we have refrained from providing T dependences for the Φ's. But there are temperature dependences in the literature, which could be incorporated in our formulation (Atkinson et al., 2006; Troe, 2007; Sander et al., 2011). Below we will incorporate such a temperature dependence in Φ_{rad} to test the sensitivity of the corresponding photolysis frequencies of CH_2O to the vertical temperature profile.

In addition the question of line structure in Φ_{rad} needs eventually to be resolved.

Of major interest to the atmospheric chemist is the impact of this new formulation of Φ on the atmospheric photolysis frequencies of CH_2O. That photolysis frequency j is given by:

$$j = \int_0^\infty \Phi(\lambda)\,\sigma(\lambda)\,F_\lambda(\lambda)\,\mathrm{d}\lambda \tag{9}$$

i.e. it also depends on the absorption cross-section, $\sigma(\lambda)$, of CH_2O, and the local actinic photon flux density $F_\lambda(\lambda)$. For our calculations of j we will use the absorption spectrum measured by Gratien et al. (2007). It is, by the way, also slightly temperature dependent; the respective function can be found in Röth et al. (1997). The atmospheric actinic photon flux density consists of down-welling and up-welling contributions, and depends of course on the solar zenith angle and altitude. It was calculated by the radiative transfer program ART (Röth, 2002) using the extraterrestrial solar flux from WMO (1985). All three factors under the integral strongly vary with wavelength, λ. (To various degrees they also vary with altitude.) As an example Fig. 4 shows $\sigma(\lambda)$, $F_\lambda(\lambda)$, and $\Phi_{mol}(\lambda)$ at 30 km altitude and 33° solar zenith angle. We particularly notice the sharp cutoff in $F_\lambda(\lambda)$ around λ = 320 nm caused by the absorption of solar UV in the ozone layer at lower wavelengths. This means that below 30 km altitude the exact form of the Φ_j at $\lambda < 300$ nm has little influence on the various photolysis frequencies. Figure 4 further indicates how much the long-wave decrease of Φ_{mol} is shifted towards longer wavelengths at the air density at 30 km altitude. In fact, this shift is so large that the

long-wave cutoff of the integrand in Eq. (9) is no longer determined by Φ_{mol}, as it is at low altitudes, but rather by the absorption spectrum of CH_2O. Hence, at altitudes above 30 km the exact form of the decrease in Φ_{mol} and Φ_{tot} at the longer wavelengths has no influence on the respective photolysis frequencies.

Given the Φ_i from Eqs. (11) to (13), $\sigma(\lambda)$ from Gratien et al. (2007) along with vertical temperature and density profiles of the US standard atmosphere (NOAA, 1976) we can calculate the vertical profiles of the photolysis rates. They are shown in Fig. 5. The shaded areas mark the 1σ error bounds of the j_i profiles based on the errors of the fitting parameters for Φ_i given in Sect. 5. As to be expected, all j_i increase with altitude. In the case of j_{rad} that increase is essentially due to the vertical change in $F_\lambda(\lambda)$, since our Φ_{rad} is neither temperature nor pressure dependent and thus independent of altitude, and the slight temperature dependence of $\sigma(\lambda)$ makes a minor contribution only. j_{tot} and j_{mol}, however, are significantly modified by the density dependence in Φ_{mol}.

In Fig. 5 we also demonstrate the impact of a possible temperature dependence in Φ_{rad}. The temperature dependence is introduced by adding the term $(300-T)\,(3k/hc)$ in the appropriate dimensional units to $1/\lambda$ in the first term of Eq. (3) (see Troe, 2007, and Sect. 2).

$$\Phi_{rad} = \frac{0.74}{1+\exp\left(\frac{-\left(1/\lambda+(300-T)\left(3k/hc\right)-1/327.4\right)}{5.4\times10^{-5}}\right)} - \frac{0.40}{1+\exp\left(\frac{-\left(1/\lambda-1/279.0\right)}{5.2\times10^{-5}}\right)} \quad (10)$$

That means: only the long-wave decay in Φ_{rad} is considered to be temperature dependent. Here k is the Boltzmann constant, h the Planck constant, and c the speed of light. As Fig. 5 shows a temperature dependence of this size clearly has a significant impact on j_{rad} and by virtue of $\Phi_{mol} = \Phi_{tot} - \Phi_{rad}$ also on j_{mol}. The effect is largest at around 15 km, the height of the temperature minimum, and about −9 % for j_{rad}, respectively ca. +6 % for j_{mol}. The temperature at 15 km is 220 K, i.e. the temperature shifts in j_{rad} and j_{mol} correspond to a temperature difference of 80 K. Apparently a correct formulation

of the T dependence of Φ_{rad} could lead to a significant improvement in the predicted vertical profiles of j_{rad} and j_{mol}.

j_{tot} remains unaffected by the proposed temperature dependency. In fact, even assuming a temperature dependence of the kind above for the long-wave decay of Φ_{tot} would have comparatively little impact on the j_{tot} profile. It would be masked by the air density dependence of Φ_{tot}: just as at lower densities, the exact form of the long-wave decay in Φ_{tot} no longer influences j_{tot}, so can its temperature dependence no longer influence j_{tot}.

Finally, in Fig. 6, we compare the photolysis frequencies based on this work's quantum yields to those calculated with the quantum yields recommended by IUPAC (2006) and JPL (Sander et al., 2011). The JPL recommendation includes an explicit temperature dependence for Φ_{rad}. In addition, both, JPL and IUPAC (2006), treat the density dependence of Φ_{mol} in terms of atmospheric pressure, which introduces a further temperature dependence. Both temperature effects are included in the calculation of the respective j_i profiles. The comparison demonstrates that even at present – without a representation of the temperature dependence – our Φ_i provide vertical profiles of the photolysis frequency which agree well with those based on Φ_i from the JPL recommendation – for all j_i and both solar zenith angles considered. The comparison with the data from Atkinson et al. (2006) is less favorable, especially for j_{mol}. This reflects the differences between $\Phi_{mol}(\lambda)$ given here and that recommended by JPL on the one hand to that recommended by Atkinson et al. (2006) on the other, which were already apparent in Figs. 2 and 3. The new quantum yields recommended by IUPAC in 2013 give photolysis rates which lie slightly above our curves for j_{mol}, just outside the error bounds.

Although the derived j_i profiles as well as the fits to the measured Φ_i (Figs. 1–3) based on the JPL recommendation and on the present work appear reasonably equivalent, we feel our formalism to be advantageous: since it consistently formulates the wavelength dependence of Φ_i in terms of $1/\lambda$, its fitting parameters are in units of energy, and represent, or are close to, molecular parameters, notably threshold

energies, which are often available and can serve as guides. Moreover, the formulation in units of energy makes it easy to introduce temperature dependences should future measurements or theoretical considerations demand it. For the same reasons our formalism should provide a useful template for the formulation of the Φ_i for the isotopologues of formaldehyde and likewise for the photolysis quantum yields of many other molecules.

The article processing charges for this open-access publication have been covered by a Research Centre of the Helmholtz Association.

References

Atkinson, R., Baulch, D. L., Cox, R. A., Crowley, J. N., Hampson, R. F., Hynes, R. G., Jenkin, M. E., Rossi, M. J., Troe, J., and IUPAC Subcommittee: Evaluated kinetic and photochemical data for atmospheric chemistry: Volume II – gas phase reactions of organic species, Atmos. Chem. Phys., 6, 3625–4055, doi:10.5194/acp-6-3625-2006, 2006.

Bowman, J. M. and Shepler, B. C.: Roaming radicals, Annu. Rev. Phys. Chem., 62, 531–553, 2011.

Christoffel, K. M. and Bowman, J. M.: Three reaction pathways in the H + HCO → H_2 + CO Reaction, J. Phys. Chem. A, 113, 4138–4144, 2009.

Gorrotxategi Carbajo, P., Smith, S. C., Holloway, A.-L., Smith, C. A., Pope, F. D., Shallcross, D. E., and Orr-Ewing, A. J.: Ultraviolet photolysis of HCHO: absolute HCO quantum yields by direct detection of the HCO Radical photoproduct, J. Phys. Chem. A, 112, 12437–12448, 2008.

Gratien, A., Picquet-Varrault, B., Orphal, J., Perrandin, E., Doussin, J.-F., and Flaud, J.-M.: Laboratory intercomparison of the formaldehyde absorption cross sections in the infrared (1660–1820 cm^{-1}) and ultraviolet (300–360 nm) spectral region, J. Geophys. Res., 112, D05305, doi:10.1029/2006JD007201, 2007.

Horowitz, A. and Calvert, J. G.: Wavelength dependence of the quantum efficiencies of the primary processes in formaldehyde photolysis at 25 °C, Int. J. Chem. Kinet., 10, 805–819, 1978.

IUPAC (2006): see Atkinson et al. (2006).

IUPAC (2013): IUPAC Task Group on Atmospheric Chemical Kinetic Data Evaluation – Data Sheet P1, available at: http://iupac.pole-ether.fr (last access: 16 January 2015) , 2013.

Miller, R. G. and Lee, E. K. C.: Single vibronic level photochemistry of formaldehydes in the A^1A_2 state: radiative and non radiative processes in H_2CO, HDCO, and D_2O, J. Chem. Phys., 68, 4448–4464, 1978.

Moortgat, G. K., Slemr, F., Seiler, W., and Warneck, P.: Photolysis of formaldehyde: relative quantum yields of H_2 and CO in the wavelength range 270–360 nm, Chem. Phys. Lett., 54, 444–447, 1978.

Moortgat, G. K. and Warneck, P.: CO and H_2 quantum yields in the photodecomposition of formaldehyde in air, J. Chem. Phys., 70, 3639–3651, 1979.

Moortgat, G. K., Seiler, W., and Warneck, P.: Photodissociation of HCHO in air: CO and H_2 quantum yields at 220 K and 300 K, J. Chem. Phys., 78, 1185–1190, 1983.

Nelder, J. A. and Mead, R.: A simplex method for function minimization, Comput. J., 7, 308–313, 1965.

NOAA: US Standard Atmosphere, NOAA-S/T76-1562, Washington D.C., 1976.

Röth, E.-P.: Description of the anisotropic radiation transfer model ART to determine photodissociation coefficients, Ber. Forschungszentrum Jülich, Jül-3960, Jülich, 2002.

Röth, E.-P., Ruhnke, R., Moortgat, G., Meller, R., and Schneider, W.: UV/VIS absorption cross sections and quantum yields for use in photochemistry and atmospheric modeling. Part 2: organic substances, Ber. Forschungszentrum Jülich, Jül-3341, Jülich, 1997.

Sander, S. P., Friedl, R. R., Abbatt, J. P. D., Barker, J. R., Burkholder, J. B., Golden, D. M., Kolb, C. E., Kurylo, M. J., Moortgat, G. K., Wine, P. H., Huie, R. E., and Orkin, V. L.: Chemical kinetics and photochemical data for use in atmospheric studies, Evaluation number 17, JPL-Publication 10-6, Pasadena, 2011.

Smith, G. D., Molina, L. T., and Molina, M. J.: Measurement of radical quantum yields from formaldehyde photolysis between 269 and 339 nm, J. Phys. Chem. A, 106, 1233–1240, 2002.

Tatum Ernest, C., Bauer, D., and Hynes, A. J.: Radical quantum yields from formaldehyde photolysis in the 30 300–32 890 cm^{-1} (304–329 nm) spectral region: detection of radical products using pulsed laser photolysis – pulsed laser induced fluorescence, J. Phys. Chem. A, 116, 6983–6995, 2012.

Terentis, A. C., Waugh, S. E., Metha, G. F., and Kable, S. H.: HCO (N, K_a, K_c, J) distributions from near-threshold photolysis of H_2CO (J, K_a, K_c), J. Chem. Phys., 108, 3187–3198, 1998.
Troe, J.: Analysis of quantum yields for the photolysis of formaldehyde at $\lambda > 310$ nm, J. Phys. Chem. A, 111, 3868–3874, 2007.
WMO: Atmospheric Ozone 1985, Vol. 1, WNO Report 16, Genf, 1985.

Table 1. Coefficients of the quantum yield function for the radical channel and 1σ errors of Eq. (3).

Coefficient	value	error
A_l	0.72	±0.01
$\lambda_{0,l}$	328.0 nm	±0.6 nm
b_l	5.2×10^{-5} nm^{-1}	$\pm 0.6 \times 10^{-5}$ nm^{-1}
A_s	0.38	±0.03
$\lambda_{0,s}$	278.4 nm	±0.8 nm
b_s	4.7×10^{-5} nm^{-1}	$\pm 1.1 \times 10^{-5}$ nm^{-1}

Table 2. Coefficients of the total quantum yield function and 1σ errors of Eq. (6).

Coefficient	value	error
A_l	1.0	fixed
$\lambda_{0,l}$	347.1 nm	±0.7 nm
b_l	5.7×10^{-5} nm^{-1}	$\pm 0.8 \times 10^{-5}$ nm^{-1}
A_s	0.20	±0.01
$\lambda_{0,s}$	284.3 nm	±0.9 nm
b_s	3.5×10^{-5} nm^{-1}	$\pm 1.4 \times 10^{-5}$ nm^{-1}

Table 3. Coefficients of the quantum yield function for the molecular channel and 1σ errors of Eq. (8).

Coefficient	value	error
A_l	1.0	fixed
$\lambda_{0,l}$	345.2 nm	±0.8 nm
b_l	6.2×10^{-5} nm^{-1}	$\pm 1.7 \times 10^{-5}$ nm^{-1}
A_m	0.75	±0.03
$\lambda_{0,m}$	325.3 nm	±0.6 nm
b_m	3.9×10^{-5} nm^{-1}	$\pm 0.5 \times 10^{-5}$ nm^{-1}
A_s	0.24	±0.05
$\lambda_{0,s}$	274.2 nm	±3.3 nm
b_s	2.3×10^{-5} nm^{-1}	$\pm 2.1 \times 10^{-5}$ nm^{-1}

Table 4. Recommended quantum yield functions for use in atmospheric chemistry models (wavelength λ in nm).

$$\Phi_{rad} = \frac{0.74}{1 + \exp\left(\frac{-\left(1/\lambda - 1/327.4\right)}{5.4\times10^{-5}}\right)} - \frac{0.40}{1 + \exp\left(\frac{-\left(1/\lambda - 1/279.0\right)}{5.2\times10^{-5}}\right)} \quad (11)$$

$$\Phi_{tot} = \frac{1}{1 + \exp\left(\frac{-\left(1/\lambda - 1/346.9\right)}{5.4\times10^{-5}}\right)\left(M/M_0\right)} - \frac{0.22}{1 + \exp\left(\frac{-\left(1/\lambda - 1/279.0\right)}{5.2\times10^{-5}}\right)} \quad (12)$$

$$\Phi_{mol} = \frac{1}{1 + \exp\left(\frac{-\left(1/\lambda - 1/346.9\right)}{5.4\times10^{-5}}\right)\left(M/M_0\right)} - \frac{0.74}{1 + \exp\left(\frac{-\left(1/\lambda - 1/327.4\right)}{5.4\times10^{-5}}\right)} + \frac{0.18}{1 + \exp\left(\frac{-\left(1/\lambda - 1/279.0\right)}{5.2\times10^{-5}}\right)} \quad (13)$$

Table 5. Coefficients and 1σ errors of the equations in Table 4, along with the coefficients of determination c for the quantum yield functions. These parameters result from a global fit of all data, as described in Sect. 5.

	coefficient	value	error
Φ_{rad}	A_l	0.74	±0.01
$c = 0.904$	$\lambda_{0,l}$	327.4 nm	±0.5 nm
	b_l	5.4×10^{-5} nm^{-1}	$\pm0.5 \times 10^{-5}$ nm^{-1}
	A_s	0.40	±0.04
	$\lambda_{0,s}$	279.0 nm	±1.3 nm
	b_s	5.2×10^{-5} nm^{-1}	$\pm2.4 \times 10^{-5}$ nm^{-1}
Φ_{tot}	A_l	1.0	fixed
$c = 0.951$	$\lambda_{0,l}$	346.9 nm	±0.5 nm
	b_l	5.4×10^{-5} nm^{-1}	$\pm0.3 \times 10^{-5}$ nm^{-1}
	A_s	0.22	±0.02
	$\lambda_{0,s}$	279.0 nm	±1.3 nm
	b_s	5.2×10^{-5} nm^{-1}	$\pm2.4 \times 10^{-5}$ nm^{-1}
Φ_{mol}	A_l	1.0	fixed
$c = 0.934$	$\lambda_{0,l}$	346.9 nm	±0.5 nm
	b_l	5.4×10^{-5} nm^{-1}	$\pm0.3 \times 10^{-5}$ nm^{-1}
	A_m	0.74	±0.01
	$\lambda_{0,m}$	327.4 nm	±0.5 nm
	b_m	5.4×10^{-5} nm^{-1}	$\pm0.5 \times 10^{-5}$ nm^{-1}
	A_s	0.18	±0.02
	$\lambda_{0,s}$	279.0 nm	±1.3 nm
	b_s	5.2×10^{-5} nm^{-1}	$\pm2.4 \times 10^{-5}$ nm^{-1}

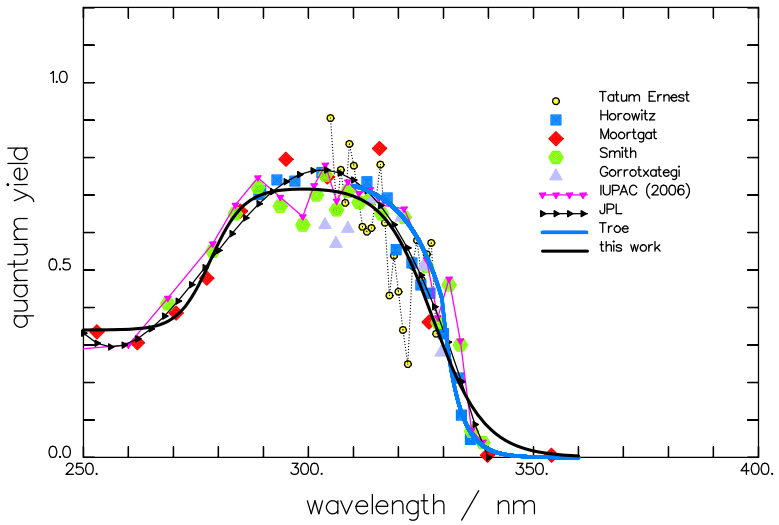

Figure 1. Spectrum of the quantum yield of the radical channel of the CH_2O photolysis at room temperature. Measured data used for the fit are indicated by the large full symbols (Horowitz and Calvert, 1978; Moortgat et al., 1983; Smith et al., 2002; Gorrotxategi Carbajo et al., 2008). The present fit and the theoretical curve from Troe (2007) are given by full lines. Recommended data are represented by small symbols connected by a thin line: JPL (Sander et al., 2011); IUPAC (2006). The line structure observed by Tatum Ernest et al. (2012) is indicated by open circles and a dotted line.

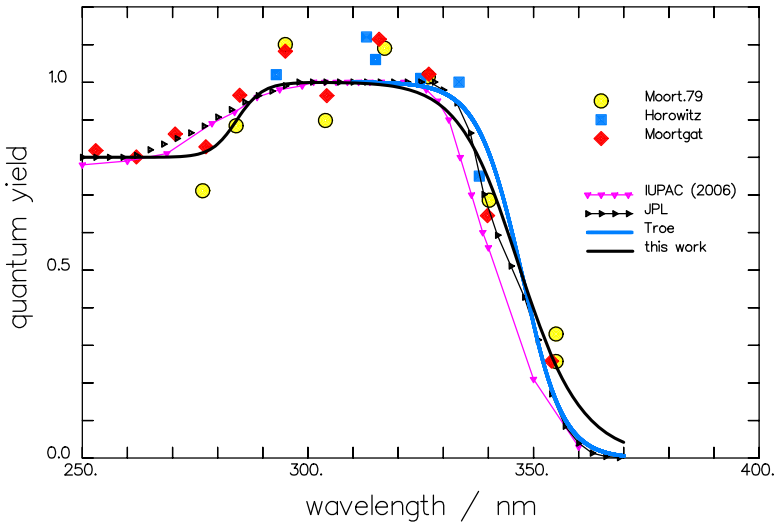

Figure 2. Spectrum of the quantum yield of the total CH_2O photolysis at room temperature. Measured data used for the fit are indicated by the large full symbols (Moort.79: Moortgat and Warneck, 1979, Horowitz and Calvert, 1978; Moortgat et al., 1983). The present fit and the theoretical curve from Troe (2007) are given by full lines. Recommended data are represented by small symbols connected by a thin line: JPL (Sander et al., 2011); IUPAC (2006).

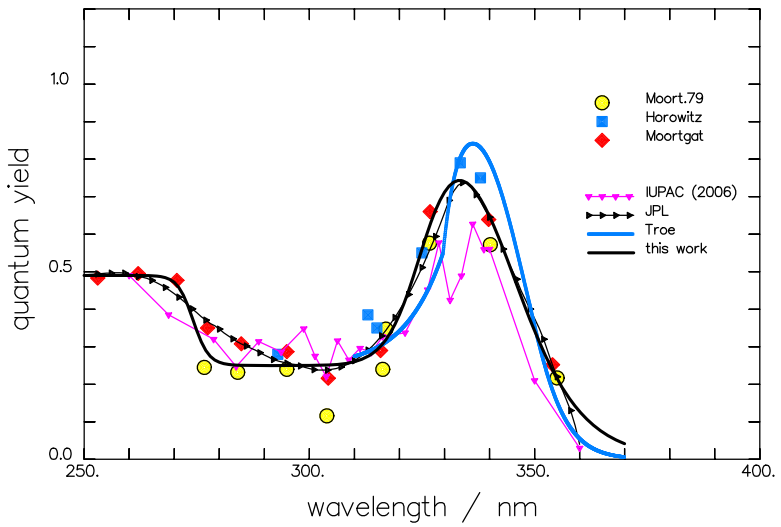

Figure 3. Spectrum of the quantum yield of the molecular branch of the CH_2O photolysis at room temperature. Measured data used for the fit are indicated by the large full symbols (Moort.79: Moortgat and Warneck, 1979, Horowitz and Calvert, 1978; Moortgat et al., 1983). The present fit and the theoretical curve from Troe (2007) are given by full lines. Recommended data are represented by small symbols connected by a thin line: JPL (Sander et al., 2011); IUPAC (2006).

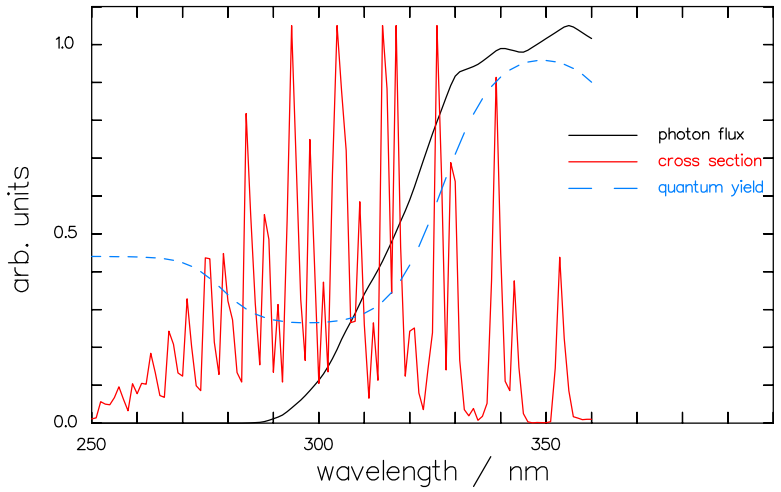

Figure 4. Spectra of the actinic photon flux density (WMO, 1985), the optical absorption cross section (Gratian et al., 2007) and the quantum yield Φ_{mol} at 30 km altitude, 33° solar zenith angle, 227 K.

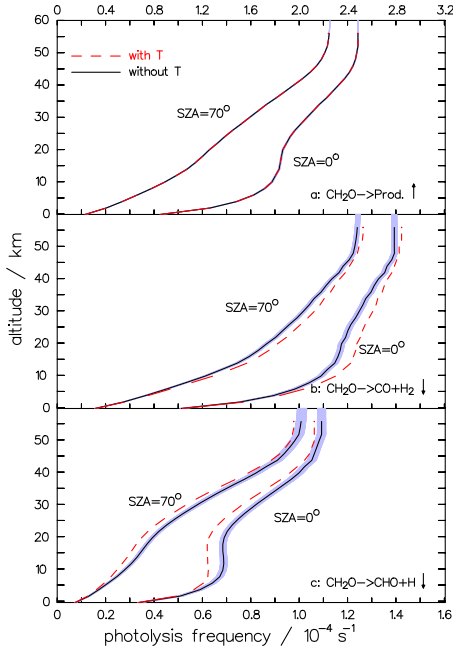

Figure 5. Impact of a temperature dependent quantum yield, Φ_{rad}, on the altitudinal profile of the photolysis of formaldehyde: total photolysis **(a)**, molecular channel **(b)**, and radical channel **(c)**. The dashed line indicates the impact of the temperature dependence of Φ_{rad} given by Troe (2007). The shaded areas mark the 1σ error bounds of the profiles based on the errors of the fitting parameters for the present quantum yields. The frequencies are depicted for two solar zenith angles (SZA). (The arrows point to the related ordinate).

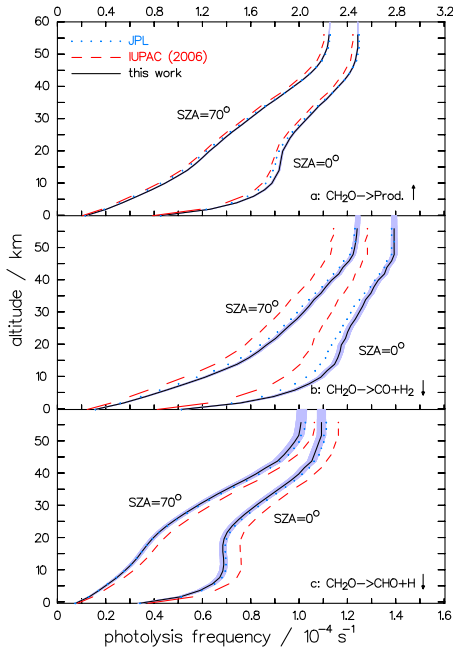

Figure 6. Comparison of the altitudinal profiles of the photolysis frequencies of formaldehyde from JPL (Sander et al., 2011); IUPAC (2006) and the present work: total photolysis **(a)**, molecular channel **(b)**, and radical channel **(c)**. The frequencies are depicted for two solar zenith angles (SZA). The shaded areas mark the 1σ error bounds of the profiles based on the errors of the fitting parameters for the present quantum yields. (The arrows point to the related ordinate).